

Flammability of Polystyrene Layered Silicate (Clay) Nanocomposites: Carbonaceous Char Formation

Alexander B. Morgan^{1†}, Richard H. Harris Jr.¹, Takashi Kashiwagi¹, Leonard J. Chyall²,
and Jeffrey W. Gilman^{1*}

¹Fire Research Division, Building and Fire Research Laboratory, National Institute of Standards and Technology, ³Gaithersburg, MD 20899-8665, USA

²Great Lakes Chemical Corporation, West Lafayette, IN 47996-2200, USA

Polymer layered-silicate (clay) nanocomposites have not only the unique advantage of reduced flammability, but also improved mechanical properties. This is a key advantage over many flame retardants, which reduce flammability but also reduce the mechanical properties of the polymer. In our efforts to further understand the mechanism of flame retardancy with polymer-clay nanocomposites, we investigated the effect of the clay, the loading level and polymer melt viscosity on the flammability of polystyrene-clay nanocomposites. The nanoscale dispersion of the clay in the polymer was analysed by wide-angle X-ray diffraction (XRD) and transmission electron microscopy (TEM). Cone calorimetry and gasification studies were used to evaluate the flammability of these nanocomposites. There were major reductions in peak heat release rates (HRRs), and increased carbonaceous char formation, for these nanocomposites. It was determined that while the viscosity of the PS nanocomposite played a role in lowering the peak HRR, the clay loading level had the largest effect on peak HRR. Finally, it was found that clay catalysed carbonaceous char formation, and the reinforcement of the char by the clay was responsible for the lowered flammability of these nanocomposites. Published in 2002 by John Wiley & Sons, Ltd.

INTRODUCTION

Polymer-clay nanocomposites have attracted a great deal of interest due to their improved mechanical, thermal, and flammability properties.^{1–5} More recent work in our laboratory has shown that polymer-clay nanocomposites exhibit reduced flammability and improved physical properties at low cost.^{6–9} A wide variety of polymer resins have been used to synthesize polymer-clay nanocomposites. This has been accomplished by the addition of an organically treated clay to a polymerization reaction (*in situ* method),^{10–14} to a solvent-swollen polymer (solution blending),¹⁵ or to a polymer melt (melt blending).^{1,5,16–18} Some of our recent work has investigated nanocomposites made with polystyrene (PS) via melt blending. The polystyrene nanocomposites were montmorillonite (MMT) clay nanocomposites, in which the sodium cations on the MMT had been replaced with organic ammonium salts. These organic ammonium salts served as the organic treatment for the clay, making the normally hydrophilic clay hydropho-

bic. This allowed the polymer to wet the surface of the clay and disperse the clay into the polymer.

The focus of our research on these PS nanocomposites was to develop a fundamental understanding of the fire retardant (FR) mechanism provided by the clay. We focused on comparing the flammability properties of: (1) nanocomposites with different MMT loading levels, and (2) nanocomposites with different melt viscosity; this was controlled by using different polymer molecular weights.⁸

EXPERIMENTAL[†]

Nanocomposite preparation

PS-montmorillonite nanocomposites (PS/MMT) were prepared on a twin-screw extruder. PS of two different M_n^s (M_n 170 000, Styron 663 and M_n 100 000 XU70262.08) were compounded with organic treated MMT from Southern Clay Products (Cloisite 20A)

*Correspondence to: J.W. Gilman, Fire Research Division, Building and Fire Research Laboratory, National Institute of Standards and Technology, Gaithersburg, MD 20899-8652, USA.

†Current address: Dow Chemical, Midland, MI.

‡This work was carried out by the National Institute of Standards and Technology (NIST), an agency of the US government, and by statute is not subject to copyright in the United States.

§According to ISO 31-8, the term 'molecular weight' has been replaced by 'relative molecular mass', symbol M_r . Thus, if this nomenclature and notation were used here, $M_{r,n}$ instead of the historically conventional M_n for the average molecular weight (with similar notation for M_w , M_z , M_v) would be used. It would be called the 'number average relative molecular mass'. The conventional notation, rather than the ISO notation, has been employed here.

¶Certain commercial equipment, instruments, materials or companies are identified in this paper in order to adequately specify the experimental procedure. This in no way implies endorsement or recommendation by NIST

Contract/grant sponsor: Flammability of Polymer-Clay Nanocomposites Consortium

using a Berstorff ZE-25 co-rotating twin-screw extruder ($L/D=35$) at 170°C with a nominal screw speed of 20.9 rad/s (200 rpm). The material was extruded at a rate of 250 g/min and the extruded strands were cooled in a water bath and pelletized with a Conair Jetro model 3045/0-9478 pelletizer (25 mm, at 205°C). The formulations prepared are shown in Table 1.

Thermal and molecular weight degradation analysis

Thermogravimetric analysis (TGA) data were collected using a TA Instruments 2950. The materials were tested under N_2 from 30°C to 700°C at a heating rate of 10°C/min . Conventional gel permeation chromatography (GPC) data were collected on a Waters Alliance 2690 equipped with a Viscotek LR40 Laser Refractometer. The column set consisted of four $300 \times 7.5\text{ mm}$ PLGel 5 micron columns (10000, 1000, 500 and 100 \AA) in series. The mobile phase was THF at a flow rate of 1 ml/min . The calibration curve was set up using narrow polystyrene standards, available from American Polymer Standards, with the following molecular weights: 675 000, 350 000, 212 000, 115 000, 30 300, 17 000, 9000, 3600, 2100 and 162. Samples and standards were dissolved in THF at 2 mg/ml .

Injection molding procedure

Disks ($7.5\text{ cm diameter} \times 0.8\text{ cm thick}$) for the cone calorimeter were prepared using an injection molding machine (Glucol LP20B semiautomatic, pneumatic). The molding machine was rated at $18.1 \times 10^3\text{ kg}$ (20 tons) with 689.5 kPa (100 psi) air pressure. The nozzle and melt chamber (barrel) theoretically held 62.4 g of melt. All resins were dried for 2 h at 75°C , and kept in a desiccator over a desiccant until they were added to the injection molding machine. An effort was made to process the resins at as low a temperature and with as short a residence time as possible to avoid degradation. The resin shot was manually added to the barrel of the injection molding machine and packed into the melt chamber. Approximately 1 min before the injection time, the resin was packed two more times for 10 s each. After each injection another shot was added to the barrel and the process repeated. A timer was used to determine when it was time to inject, and filling of the barrel was done immediately after an injection to keep the residence time as equal as possible for each disk. Table 2 shows the specific injection molding conditions for the individual polystyrenes.

Table 1. PS formulations^a

High M_n PS	Low M_n PS	Clay (SCPX2197)
98	–	2
95	–	5
90	–	10
–	98	2
–	95	5
–	90	10

^aMass fraction %.

Table 2. Injection molding of polystyrene

Clay identity	Mass fraction % clay	Process temp. ($^{\circ}\text{C}$)	Injection pressure (kPa)
Blank (low MN PS)	0	210	689
SCPX2197	2	210	689
SCPX2197	5	210	689
SCPX2197	10	210	689
Blank (high MN PS)	0	210	689
SCPX2197	2	225	689
SCPX2197	5	210	689
SCPX2197	10	200	689

Nanoscale clay dispersion characterization

XRD data were collected on powder specimens with a Philips diffractometer using $\text{Cu K}\alpha$ radiation ($\lambda=0.1505945\text{ nm}$) with a $0.02\ 2\theta$ step size and a 2 s count time. Bright-field TEM images of PS nanocomposites were obtained at 120 kV , at low dose conditions, with a Philips 400 T electron microscope. All samples were ultramicrotomed with a diamond knife on a Leica Ultracut UCT microtome at room temperature to give sections with a nominal thickness of 70 nm . The sections were transferred from water to carbon-coated Cu grids of 200 mesh ($127\ \mu\text{m}$).

Cone calorimetry

Cone calorimeter experiments were performed at an incident heat flux of 50 kW/m^2 using the cone heater.¹⁹ Peak heat release rate (HRR), mass loss rate (MLR), specific extinction area (SEA), ignition time (t_{ign}), carbon monoxide yield, carbon dioxide yield, and specific heat of combustion data are reproducible to within $\pm 10\%$ when measured at 50 kW/m^2 flux. The cone data reported here are the average of three replicated experiments. The specific errors (one sigma) are shown as error bars on the plots of the cone data.

Gasification

The gasification device built at NIST is shown schematically in Fig. 1. The cylindrical chamber was 0.61 m in diameter and 1.70 m in height. Two windows provided optical access. The chamber walls were water-cooled to 25°C . Products and ambient gases were removed via an exhaust duct, and a constant nitrogen flow of 7.67 l/s at 25°C was maintained during the experiments. The temperature of the elements in the cone-shaped heater was fixed at 808°C to maintain a constant emission spectrum for all tests. A water-cooled shutter was extended to protect the sample from the incident radiant flux during nitrogen purge, prior to testing. Flux levels varied about $8\%–10\%$ across the 0.1 m diameter sample region. The sample, 75 mm in diameter and 8 mm in thickness, was placed in an aluminium foil pan having nearly the same diameter as that of the sample, and 13 mm high side walls. The sample mass was measured with a load cell, and these data were recorded at 0.5 s intervals. The uncertainty in

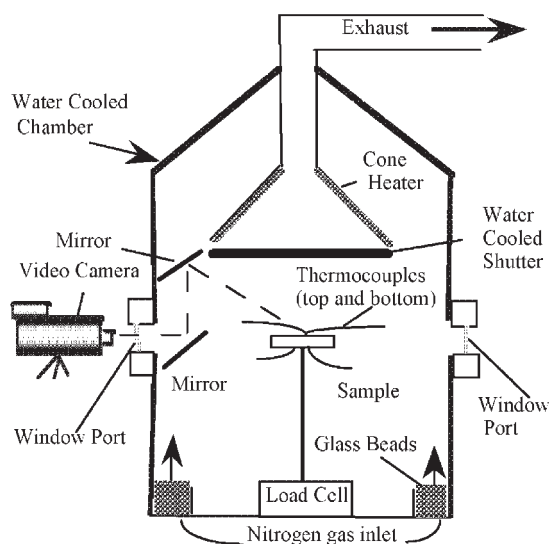


Figure 1. Schematic of gasification device.

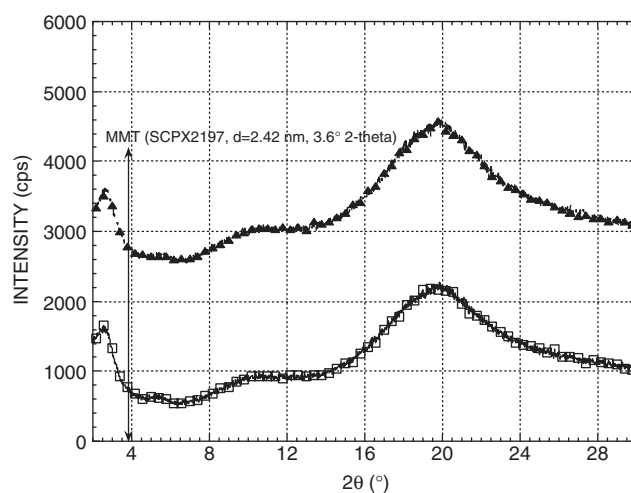


Figure 2. X-ray diffraction data for PS/5% MMT nanocomposites (high M_n 170 K and low M_n 100 K).

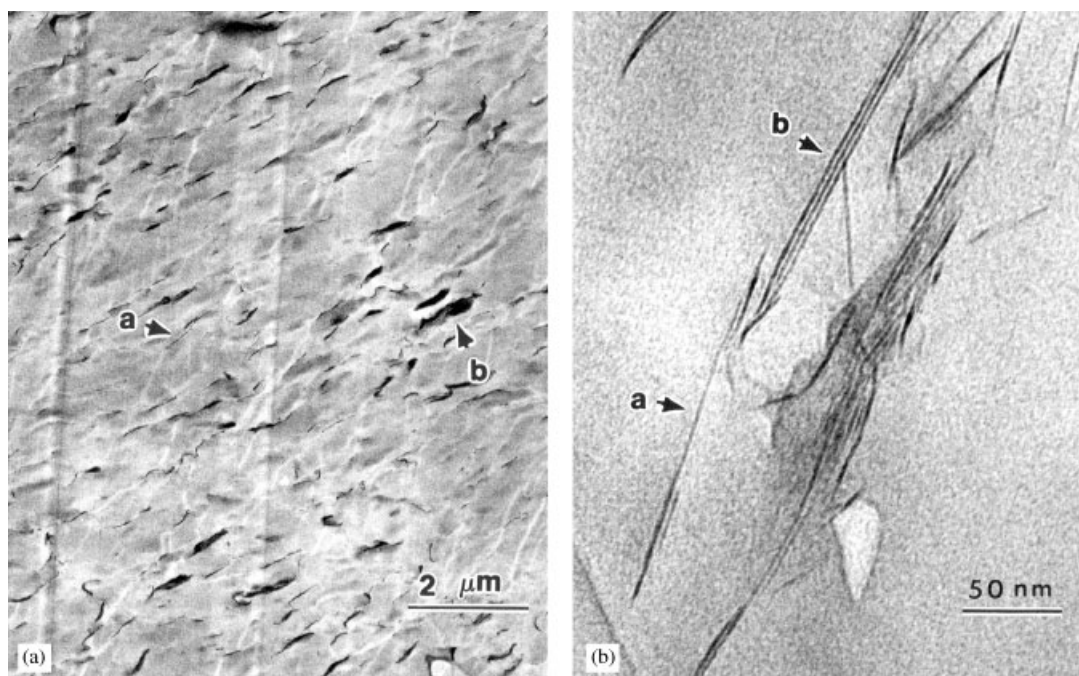


Figure 3. (A) Low magnification TEM image of PS+5% clay. Note small multi-layer tactoids (a) as well as larger tactoids (b). (B) High magnification TEM image of PS+5% clay. Single layers (a) as well as small layer stacks (b) can be observed.

the measurement of interest in the gasification data is shown in each plot as an error bar.

RESULTS AND DISCUSSION

Clay nanoscale dispersion characterization

The nanoscale dispersion of the clay in the polymer is of utmost importance, as the type of dispersion determines the mechanical and thermal properties of the nanocomposite.^{1,9,18,26} The PS/MMT nanocomposite samples, of

differing molecular weight, each containing a mass fraction of 5% of an organically treated montmorillonite clay, were analysed by XRD (Fig. 2). XRD indicated that the samples were intercalated nanocomposites. The d-spacings increased from 2.42 nm (d-spacing for organically treated clay: Cloisite 20A) to 3.27 nm and 3.34 nm for the high molecular weight and low molecular weight polystyrene samples, respectively. However, at low magnification, TEM shows that the clay is well dispersed throughout the polymer (Fig. 3A). Individual clay layers along with two and three layer particles are observed well dispersed (delaminated) in the polymer matrix (Fig. 3B). In addition, large

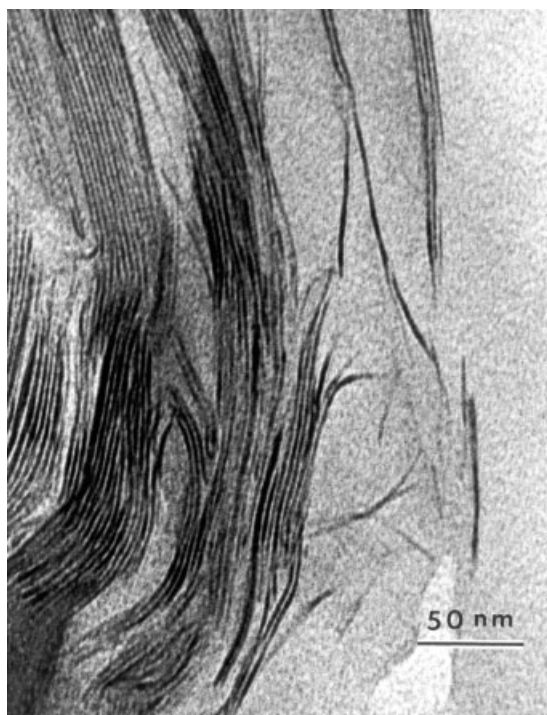


Figure 4. High magnification TEM image of PS+5% clay.

intercalated tactoids (multi-layer particles), as seen in Fig. 3A, are also visible (Fig. 4). This mixed nanomorphology reflects results seen with PS/MMT nanocomposite samples prepared previously.^{18,20} This discrepancy between XRD and TEM results is not uncommon, and has been seen for a wide range of materials. This reinforces the necessity of characterizing nanocomposites using as many methods as possible.²¹ In regard to the effects of clay dispersion on flammability, we have shown that exfoliated and intercalated nanocomposites perform equally well in the cone calorimeter.²⁷

Thermal and flammability analysis

The thermogravimetric analysis (TGA) of the PS nanocomposites is shown in Table 3. The data reveal a 19°C increase in thermal stability for both molecular weight PS/MMT samples. This is less than half of the 49°C increase in thermal stability observed previously for PS/MMT nanocomposites.²⁰ The reduced improvement in thermal stability may be due to the different processing methods used in each study. The PS/5% MMT nanocomposites here were compounded at 170°C in a 25 mm twin screw extruder exposed to air; whereas, the previous PS/MMT nanocomposites were

Table 3. TGA data of PS/5% MMT nanocomposites

Sample	TGA derivative maxima
100K M_n PS	412°C
100K M_n PS/5% MMT nanocomposite	431°C
170K M_n PS	414°C
170K M_n PS/5% MMT nanocomposite	433°C

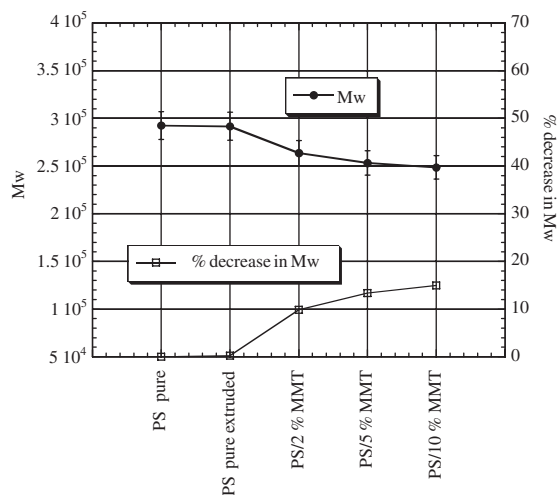


Figure 5. GPC data for high M_n PS and PS/MMT nanocomposites.

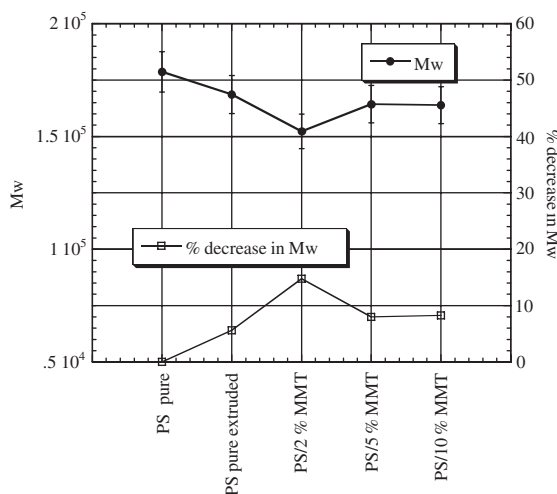


Figure 6. GPC data for low M_n PS and PS/MMT nanocomposite.

compounded at 150°C to 170°C in a mini-extruder under nitrogen.¹⁸ Indeed, GPC analysis of the samples (Figs. 5 and 6) extruded at a slightly higher temperature without a nitrogen flow in the extruder showed some evidence of degradation in the form of lower M_n . This is consistent with our observation, which found that low temperature processing was necessary to prevent PS degradation when organo-MMT was present.¹⁸ The reduction of M_n may also be due to decomposition of the organic treatment. The onset of thermal decomposition (T_{dec}) of the organic modification associated with a layered-silicate sets the upper limit on the processing temperature for preparing polymer layered-silicate nanocomposites, and for additional processing (injection or compression molding) of the nanocomposite.²² Most organic modifications for MMTs are alkyl ammonium salts, where the alkyl ammonium cation has replaced the alkali cation on the natural montmorillonite via ion exchange. However, these alkyl ammonium salts have limited thermal stability,²³ and under some processing conditions easily degrade to

tertiary amine and an α -olefin, via the Hofmann elimination,²⁴ or to alkylhalide and tertiary amine via attack of residual halide.²⁵ While the typical T_{dec} reported for an alkyl ammonium treated MMT is 200°C, decomposition could occur at lower temperatures due to prolonged exposure to air during heating of the polymer, or from thermal gradients and hot spots within the extruder.

To study the effect of melt viscosity²⁶ combined with the effect of MMT loading on the flammability of PS/MMT nanocomposite by cone calorimetry, PS/MMT nanocomposites were analysed with different M_n and MMT loading levels. The HRR data for pure PS and PS/10% MMT nanocomposites for both molecular weights are shown in Fig. 7. The factor of 3 to 4 reduction in the peak HRR for the PS/10% MMT nanocomposites compared with the pure PS is impressive. Furthermore, even though there was no statistically significant difference in the HRR of the two different molecular weights of pure PS samples, there was a significant difference in the flammability of the two different molecular weights of the PS/10% MMT nanocomposites. The high M_n nanocomposite had about a 30% lower HRR throughout the first 400 s of the combustion experiment compared with the low M_n sample. This may indicate that the viscosity of the molten degrading material in the burning nanocomposite is significantly different for the two samples, and that this has a significant effect on the rate that volatile decomposition products can escape into the gas phase. This longer residence time for decomposition products may provide the opportunity for other secondary reactions to occur, such as those which form char (see discussion of gasification below).

The HRR data for the high M_n PS/MMT nanocomposites with mass fractions of 2%, 5%, and 10% clay are shown in Fig. 8. The reduction in peak HRR improved as the mass fraction of MMT increased. The additional improvement for the PS/MMT nanocomposite with 10% MMT only occurred during the first 100 s of the burn. A levelling off of improvement in properties at 5% is a common result for many layered-silicate nanocomposites, regardless of the property.²⁷ As

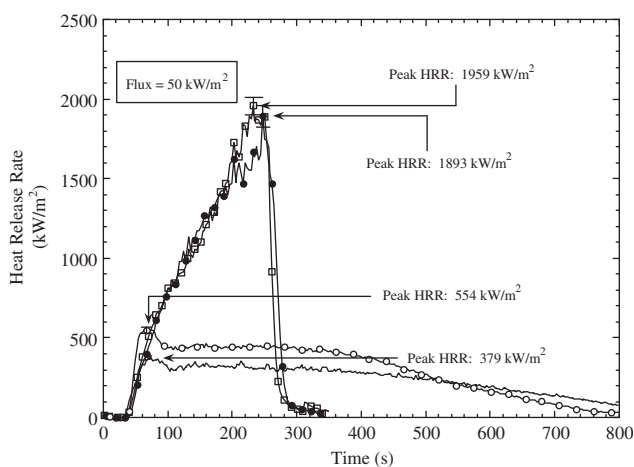


Figure 7. HRR plots for pure PS and PS/10% MMT nanocomposites (low M_n and high M_n).

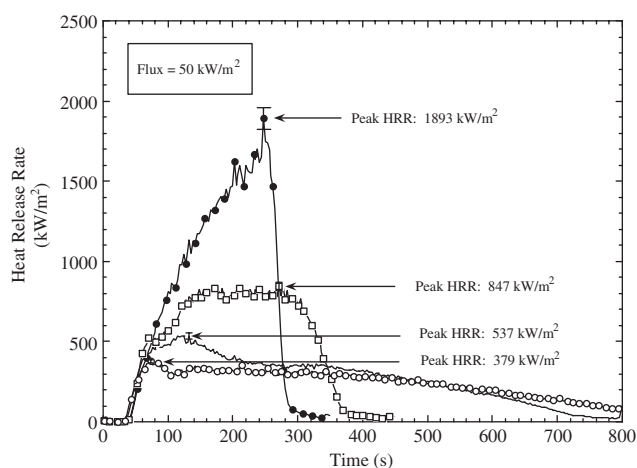


Figure 8. HRR plots for the high M_n pure PS, and the high M_n PS/MMT nanocomposites with 2%, 5%, and 10% clay loading.

impressive as the HRR data are, the data most telling of the novelty of this flame retardant approach comes from the gasification data.

The gasification device (Fig. 1) allows pyrolysis, in a nitrogen atmosphere, of samples identical to those used in the cone calorimeter, at fire like heat fluxes, without complications from gas phase combustion, such as heat feedback and obscuration of the sample surface from the flame. Typical measurements taken during a gasification experiment include mass loss rate, and a video of the sample as it undergoes gasification. The MLR data from the gasification of PS/MMT nanocomposites showed identical trends to those found in the HRR data from the cone (Figs. 7 and 8). However, the digitized video images taken during the gasification of the low M_n PS/5% MMT nanocomposite showed the most important effect of the nano-dispersed clay on the PS degradation. In contrast to the rapid-boiling liquid layer observed for the pure PS, the PS/5% MMT sample appeared to solidify and was converted to a black solid residue very early in the experiment, at 90 s (Fig. 9). Once this residue (char) formed, the MLR slowed to 25% of that for pure PS, and as stated before, it was this reduced MLR, or fuel feed rate, that was responsible for the dramatic reduction in the HRR. The video images and the gasification residue yields for the PS/MMT nanocomposites (Fig. 9) showed that the otherwise non-char forming PS was converted to a charring system by the nano-dispersed clay. The carbonaceous char yields for these PS/MMT nanocomposites are shown in Table 4. Very few other additive flame retardants are capable of causing PS alone (without a carbonific) to give carbonaceous char, especially at this low a loading and with such a dramatic reduction in flammability.

A polymer viscosity (related to polymer M_n) effect was also observed in the gasification experiments for the PS nanocomposites. The high M_n PS nanocomposite swelled, or intumesced, to a greater extent than the low M_n PS nanocomposite during the gasification and charring process. This may indicate a higher melt viscosity for the sample that swelled more, and suggests one reason that the decomposition products escaped the

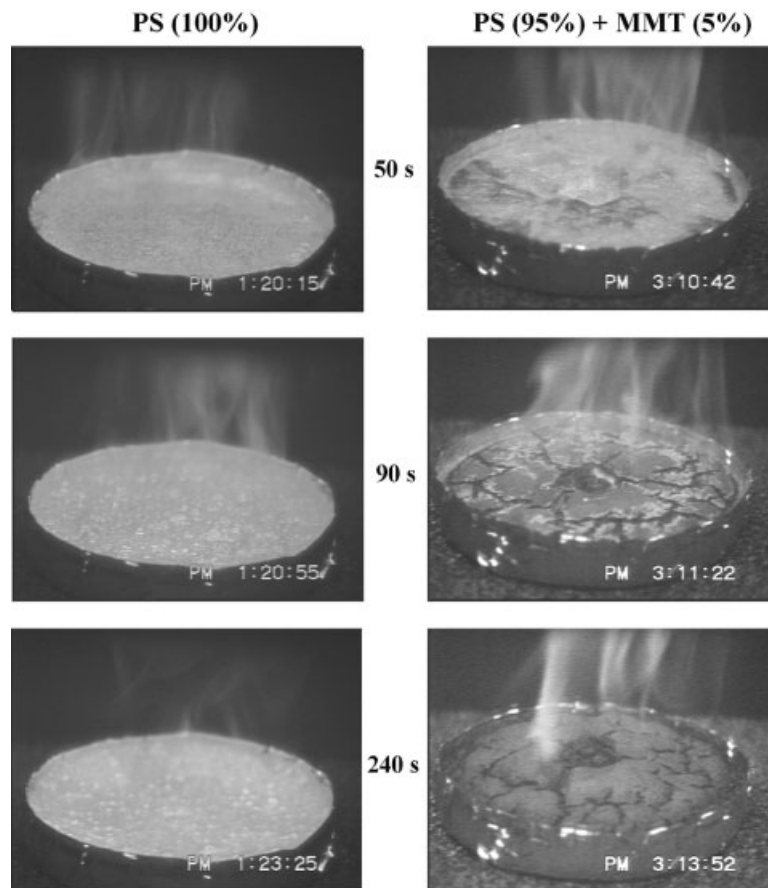


Figure 9. Digitized images from nitrogen gasification at a flux of 50 kW/m² of pure PS (low M_n) and PS/5% MMT nanocomposite (low M_n). The extensive carbonaceous char formation can clearly be observed in the nanocomposite (right) samples.

Table 4. Carbonaceous char yields for PS/MMT nanocomposites

Nanocomposite	Carbonaceous char yield ^a
PS/2% MMT	0.7%
PS/5% MMT	2.3%
PS/10% MMT	3.3%

^aThese are carbonaceous residue yields only, the silicate fraction has been subtracted out. All silicate is assumed to have survived the gasification, and the organic is assumed to have been volatilized completely. It is assumed that the carbonaceous residue is solely derived from PS.

condensed phase at a slower rate (i.e. the MLR was lower).

CONCLUSIONS

The most important result from this work is the formation of a clay-reinforced carbonaceous char during combustion of nanocomposites. This is particularly significant for polystyrene, which normally produces little or no char when burned alone. In the case of a polystyrene clay nanocomposite, char is indeed

formed, and lower HRRs result. It appears from the gasification data (videos and mass loss data) that this clay-reinforced carbonaceous char is responsible for the reduced mass loss rates and hence the lower HRRs. Specifically, the observed MLR data indicate that the clay-reinforced char layer acts as a barrier to fuel release, thus lengthening the burn times of the nanocomposite and lowering the HRR. Polymer viscosity did appear to play some role in lowering the HRR for these nanocomposites, with the high M_n material showing a 30% lower HRR when compared with the low M_n material. With regard to the effect of clay loading on the HRR for the nanocomposite, the most effective loading level was a mass fraction of 5%. There was some improvement at 10% mass fraction loadings, since the mechanical properties of this high a loading can be deleterious, such heavy loading might be counter-productive. We are currently investigating co-additives for polymer-clay nanocomposites which can lower the HRR further possibly in a synergistic manner.

ACKNOWLEDGEMENTS

We would like to thank the Flammability of Polymer-Clay Nanocomposites Consortium for funding of this work. We would also like to thank members of NIST-BFRL for their assistance in this research: Mr Michael Smith for cone calorimeter work, Ms Lori

Brassell for sample preparation and cone calorimeter data analysis, and Mr John Shields for gasification apparatus work. We would also like to thank members of NIST-MSEL for their assistance:

Dr James Cline of NIST-MSEL for use of the Ceramics Division XRD facilities, and Dr Catheryn L. Jackson for assistance with TEM work.

REFERENCES

1. Giannelis EP. *Adv. Mater.* 1996; **8**: 29.
2. Kojima Y, Usuki A, Kawasumi M. *et al. J. Mater. Res.* 1993; **8**: 1185.
3. Wang Z, Pinnavaia TJ. *Chem. Mater.* 1998; **10**: 1820.
4. Burnside SD, Giannelis EP. *Chem. Mater.* 1995; **7**: 1597.
5. Lee J, Takekoshi T, Giannelis EP. *Mat. Res. Soc. Symp. Proc.* 1997; **457**: 513.
6. Gilman JW, Kashiwagi T, Lichtenhan JD. *SAMPE J* 1997; **33**: 40.
7. Gilman JW, Kashiwagi T, Brown JET, Lomakin S, Giannelis EP, Manias E. *Proc 43rd Inter. SAMPE Symp. and Exhib. Society for Advancement of Materials & Process Engineering*: Anaheim, CA, 1998; 1053.
8. Gilman JW, Kashiwagi T, Nyden M, *et al. Chemistry and Technology of Polymer Additives*. The Royal Society of Chemistry: Cambridge, 1999, 249–265.
9. Gilman JW. *Appl. Clay Sci.* 1999; **15**: 31.
10. Fujiwara S, Sakamoto T. *Kokai Patent Application*, SHO 51(1976)-109998, 1976.
11. Lan T, Pinnavaia TJ. *Chem. Mater.* 1994; **6**: 2216.
12. Usuki A, Kato M, Okada A, Kurauchi T. *J. Appl. Polym. Sci.* 1997; **63**: 137.
13. Meier LP, Shelden RA, Caseri WR, Suter UW. *Macromolecules* 1994; **27**: 1637.
14. Reichert P, Kressler J, Thomann R, Mulhaupt R, Stoppelmann G. *Acta Polymer.* 1998; **49**: 116.
15. Jeon HG, Jung HT, Less SD, Hudson S. *Polymer Bull.* 1998; **41**: 107.
16. Maxfield M, Christiani BR, Murthy SN, Tuller H. US Patent 5,385,776 1995.
17. Fisher H, Gielgens L, Koster T. *Nanocomposites from Polymers and Layered Minerals*: TNO-TPD Report, 1998.
18. Gilman JW, Jackson CL, Morgan AB, *et al. Chem. Mater.* 2000; **12**: 1866.
19. Babrauskas V. *Fire Mater.* 1995; **19**: 243.
20. Gilman J, Kashiwagi T, Lomakin S. *et al. In Fire Retardancy of Polymers: the Use of Intumescence*, Le Bras M, Camino G, Bourbigot S, Delobel R (eds.). The Royal Society of Chemistry: Cambridge, 1998; 203–221.
21. For a complete discussion of the nanocomposite characterization issues associated with XRD and TEM see: Morgan AB, Gilman JW, Jackson CL. *Macromolecules* 2001; **34**: 2735.
22. Gilman JW, Awad WH, Davis RD, *et al. Chem. Mater.* 2002; **14**: 3776–3785.
23. Xie W, Gao Z, Pan W-P, Vaia R, Hunter D, Singh A. *Chem. Mater.* 2001; **13**: 2979–2990.
24. Saunders WH, Jr. In *Ionic Aliphatic Reactions*, Prentice-Hall: Englewood Cliffs, NJ, 1965; 67–68.
25. VanderHart DL, Asano A, Gilman JW. *Chem. Mater.* 2001; **13**: 3796.
26. This assumes $\eta \sim Mw^{0.6-0.8}$ see *Textbook of Polymer Science*, Billmeyer F (ed.). John Wiley: New York, 1984; 211.
27. Gilman JW, Kashiwagi T, Morgan AB *et al. National Institute of Standards and Technology Internal Report (NISTIR) 6531*, July 2000. NIST: Gaithersburg, MD.